

# Preparation of CuO/MgO Composite for Removal of Tartrazine in Aqueous Solution

Phan Thi Yen, Vu Anh Tuan\*

Hanoi University of Science and Technology – No. 1, Dai Co Viet Str., Hai Ba Trung, Ha Noi, Viet Nam

Received: September 06, 2017; Accepted: June 25, 2018

## Abstract

In this study, the CuO/MgO composite was prepared by co-precipitation method, as-prepared samples were characterized by SEM, TEM, XRD and  $N_2$  adsorption/desorption isotherms. The removal of tartrazine from aqueous solution by CuO/MgO/ $H_2O_2$ /UV was investigated and compared to other systems with/without  $H_2O_2$  and UV irradiation. The amount of dye removed was determined by measuring the concentration of the dye at its characteristic wavelengths by UV-Vis spectrophotometer. The removal efficiency observed was in the order: CuO/MgO/UV/ $H_2O_2$  > CuO/MgO/ $H_2O_2$  > CuO/MgO/UV > CuO/MgO > UV/ $H_2O_2$  > UV >  $H_2O_2$ . In addition, the pseudo-first order kinetic model was used for fitting the experimental data profiles in order to find the reaction rate constant.

Keywords: CuO/MgO, Removal, Tartrazine, Photocatalyst, Composite

## 1. Introduction

Recently, metal oxide nanostructure with architecture has received considerable attention due to its unique textural and physical properties and potential for many applications. Among metal oxides, cupric oxide (CuO) is a p-type semiconductor with a narrow bandgap of 1.2 eV [1]. Nano size CuO and its composites were used in various applications such as gas sensor, solar energy conversion, electrode material in lithium ion batteries, heterogeneous catalyst [2-5].

Magnesium oxide (MgO) is widely used as the adsorbent because it is abundant, nontoxic, environmental friendly material with high specific surface area and easy regeneration [6]. For removal of dyes on MgO and MgO-based materials, many studies have been reported: adsorption of reactive and vat dyes on MgO [7], removal of methyl blue dye by MgO and Ni-MgO [8], adsorption of remazol red RB-133 by  $Fe_2O_3$ /MgO [9] and methyl orange by chitosan/MgO [10], and removal of reactive blue 19 and reactive red 198 on MgO.

Nowadays, the textile and garment industries form a major part of manufacturing production, employment, and trade. It has played such an important role in economic development and contributed the most to the GDP of many developing countries. There are more than hundred thousand commercial dyes with a rough estimated production of about million tons per year [11]. Of such a huge

production the exact data on the quantity of dyes discarded in environmental is not available. It is reported that 10-15% of the used dyes enter the environment through wastes. Most of synthetic dyes are toxic, even carcinogenic and this poses a serious hazard for human being and aquatic animals [12]. To remove dyes from textile industrial wastewater, various treatment methods based on physical, chemical, biological, acoustical, radiation, and electrical processes have been adopted [13]. Among these dye removal methods, chemical oxidation method using oxidizing agents such as hydrogen peroxide, ozone, potassium permanganate with assistant of UV light is the most commonly used for removal of dye since they require low quantities and short reaction time and possibly complete degradation of dyes.

The colour additive tartrazine, whose IUPAC name is trisodium 1-(4-sulfonatophenyl)-4-(4-sulfonatophenylazo)-5-pyrazolone-3-carboxylate, the structure is shown in Fig. 1, was selected as a model of azo dye because it widely uses in food products, drugs, cosmetics, electroplating, pharmaceuticals and the textile industry. Particularly, it causes asthma, eczema, thyroid cancer, and some other behavioural problems [14,15].

In the study, MgO/CuO nanocomposite was prepared by co-precipitation method. The physical and textural properties of samples were characterized by XRD, FE-SEM, TEM, and  $N_2$  adsorption/desorption isotherm. The batch reaction was conducted to evaluate removal efficiency of as-synthesized samples under different conditions. In addition, the kinetic of reaction also was investigated.

\* Corresponding author: Tel.: +84-912911902  
Email: tuan.vuanh@hust.edu.vn

## 2. Experimental

### 2.1. Chemicals

Tartrazine (99.5 %) was purchased from Sigma-Aldrich without any purification.  $\text{Cu}(\text{NO}_3)_2 \cdot 3\text{H}_2\text{O}$  (99%) was purchased from Germany,  $\text{Mg}(\text{NO}_3)_2 \cdot 6\text{H}_2\text{O}$  (99%),  $\text{K}_2\text{CO}_3$  (99%),  $\text{H}_2\text{O}_2$  (99%),  $\text{NaOH}$  (99%),  $\text{H}_2\text{SO}_4$  (99%) were purchased from China. Distilled water was used in preparation of solutions and washing precipitation in the present study.

### 2.2. Synthesis of nanocomposite CuO/MgO

The synthesis experiment of nanocomposite MgO/CuO by precipitation method is described in Fig. 1. At room temperature, 50 mL of 0.5 M  $\text{K}_2\text{CO}_3$ , 25 mL of 0.5 M  $\text{Mg}(\text{NO}_3)_2 \cdot 6\text{H}_2\text{O}$  and 25 mL of 0.5 M  $\text{Cu}(\text{NO}_3)_2 \cdot 3\text{H}_2\text{O}$  were added equally into the 250 mL glass beaker. The final pH of solution was adjusted by  $\text{NaOH}$  up to a value between 10 and 11. The mixture was stirred for 1 h at room temperature, then moved into hydrothermal equipment (Autoclave) at 150 °C for 24 h. The precipitate was filtered and washed at least 10 times with distilled water and then dried at 100 °C for 12 h. Finally, the powder was calcined at 500 °C for 5 h with the heating rate of 1 °C/min in air in a muffled furnace.

MgO sample was prepared by the same procedure for CuO/MgO but without the addition of  $\text{Cu}(\text{NO}_3)_2 \cdot 3\text{H}_2\text{O}$ . The physical of CuO/MgO was compared to MgO. In addition, the removal of tartrazine on MgO was carried out at the same condition with CuO/MgO.

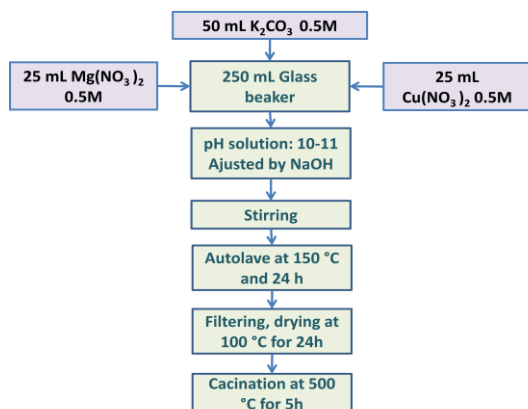


Fig. 1. Schematic synthesis of CuO/MgO

### 2.3. Catalysts Characterization of materials

The crystalline phase of as-prepared MgO/CuO was investigated by X-ray power diffraction. XRD patterns were obtained by using Bruker D8 Ax XRD-diffractometer (Germany) with  $\text{Cu K}\alpha$  irradiation (40kV, 40 mA). The  $2\theta$  ranging from 20 to 70° was selected to analyse the crystal structure. The

morphology and size of the samples were observed by transmission electron microscopy (TEM, JEM-2010) and field emission scanning electron microscopy (FE-SEM, JEOL-7600F). Textural properties were measured via  $\text{N}_2$  adsorption/desorption isotherm using a Quanta chrome instrument (Autosorb iQ, version 3.0 analyzer). The specific surface area was calculated by using the Brunauer-Emmett-Teller (BET) method and the pore size distribution was obtained by using the Barrett-Joyner-Halenda (BJH) method.

### 2.4. Photocatalytic activity of the as-synthesized materials

The photocatalytic activity of CuO/MgO sample was performed by batch reactor. At room temperature (~25°C), 0.1 g of sample was added into reactor containing 100 mL tartrazine solution of 50 mg/L and 0.03 mL  $\text{H}_2\text{O}_2$  solution of 30%. The 15 W halogen lamp was used as the UV light source. At given time intervals, an aliquot (2 mL) of dye was withdrawn from the suspension and immediately filtered by a syringe filter (0.45  $\mu\text{m}$  PTFE membrane). The dye concentration of the filtrate was analyzed by a UV-Vis spectrophotometer (Agilent 8453) at 428 nm. The removal efficiency (Re%) of the dye solution was calculated by equations (1).

$$\text{Re} (\%) = \frac{C_0 - C_t}{C_0} \times 100\% \quad (1)$$

Where  $C_0$  and  $C_t$  are the initial and time  $t$  dye concentration in solution (mg/L), respectively.

## 3. Results and discussion

### 3.1. FE-SEM and TEM analysis

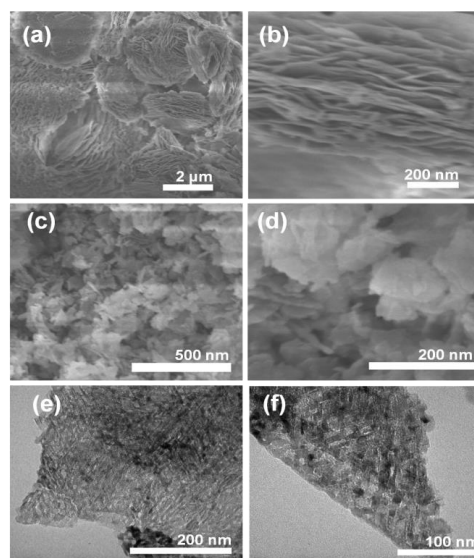


Fig. 2. (a) and (b) SEM images of MgO, (c) and (d) SEM images of CuO•MgO, (e) and (f) TEM images of CuO•MgO.

The FESEM and TEM images of MgO and CuO/MgO samples are presented in Fig. 2. The morphology of MgO particles was hierarchical flower-like with a diameter from 2-5  $\mu\text{m}$ . The flower-like particles are made up of a number of nanosheets with a thickness of 10 nm, as seen in Figs 2(a) and (b). The CuO/MgO sample exhibited the different morphology to MgO. It is observed to have agglomerates of polyhedral shape with the mean size of 200 nm, as seen in Figs 2(c) and (d). The agglomerated particles consisted of many smaller particles ranging from 10 to 15 nm in size, as seen by TEM images in Figs 2(e) and (f).

### 3.2. XRD analysis

X-ray powder diffraction of MgO and CuO/MgO composite are presented in Fig. 3. The XRD patterns of MgO shows three broad diffraction peaks at 37, 43, and 62.4°, which can be indexed to the (111), (200), (220) planes, respectively, of cubic MgO, which is in good agreement with the reported data (JCPDS data No. 78-0430) [16]. For the composite, the diffraction peaks of CuO were observed at 35.5, 38.7, 48.7, 58.3, 66.1, 68.2°. In addition, the diffraction peaks of MgO were also observed, but these peaks became broader and its intensity decreased. It indicated that CuO/MgO composite was less crystallinity compared to MgO. The average crystallite size of as-prepared samples ( $D_c$ ) were estimated using the Debye-Scherrer equation [17], expressed following:

$$D_c = \frac{K\lambda}{\beta \cos \theta} \quad (2)$$

Where  $\theta$  and  $\beta$  are the diffraction angle and the width of the observed diffraction line at its half-intensive maximum, respectively.  $\lambda$  is the X-ray wavelength (nm) and  $K$  is the shape factor. The average crystallite sizes of MgO and CuO/MgO were 8.6 and 7.2 nm, respectively, estimated from (200) plane, as shown in Table 1.

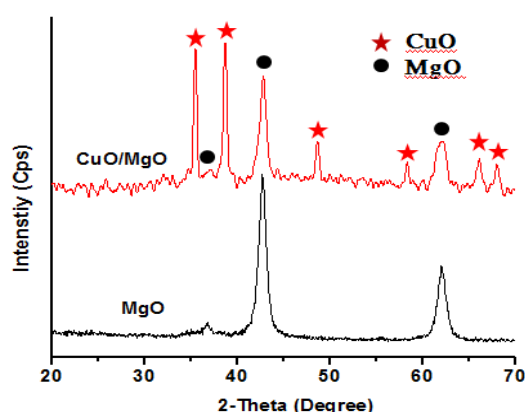


Fig. 3. XRD patterns of MgO and CuO/MgO composite.

Table 1. Textural properties of MgO and CuO/MgO composite.

Sample	$S_{\text{BET}}$ ( $\text{m}^2/\text{g}$ )	$V_{\text{pore}}$ ( $\text{cm}^3/\text{g}$ )	$D_{\text{pore}}^a$ (nm)	$D_c^b$ (nm)
MgO	132	0.263	9.3	8.6
CuO/MgO	12.8	0.038	32.4	7.2

<sup>a</sup> Average pore size

<sup>b</sup> Crystallite size

### 3.3. $\text{N}_2$ adsorption/desorption analysis

Fig. 4 presents the typical  $\text{N}_2$  adsorption/desorption isotherms and pore size distributions of as-synthesized MgO and CuO/MgO samples. The isotherm curve of MgO was classified as type II according to IUPAC classification with a  $H_4$  hysteresis loop indicating a porous material. The pore size distribution concentrated on 4-10 nm. The average pore diameter and BET surface area were 9.3 nm and 132  $\text{m}^2/\text{g}$ , respectively. For CuO/MgO composite, the hysteresis loop, pore volume and surface area were much smaller than those of MgO, this can be ascribed to sintering of copper hydroxyl during the calcinations process. However, the pore size distribution of CuO/MgO was comparatively concentrated in large size at around 17-22 nm. The average pore diameter and BET surface area were 32.4 nm and 12.8  $\text{m}^2/\text{g}$ , respectively, as shown in Table 1.

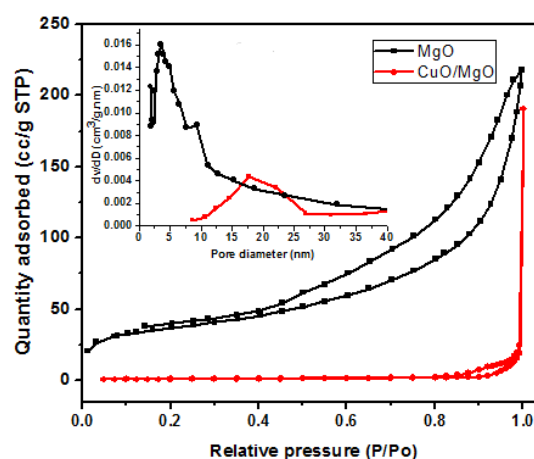


Fig. 4.  $\text{N}_2$  adsorption/desorption isotherms (inset: pore size distributions) of MgO and CuO/MgO composite.

### 3.4. UV-Vis spectra of removal of tartrazine

The activity of CuO/MgO composite for removal of tartrazine was investigated by conducting a number of experiments in the present of  $\text{H}_2\text{O}_2$  under UV light. Fig. 5 exhibits independent of adsorption spectrum of tartrazine on time. It is evidently seen

that the absorbance intensity decreased gradually with time. It indicated that 72.1% tartrazine decomposed in 80 min under UV illumination.

In tartrazine spectrum before oxidation ( $t = 0$ ), the absorption spectrum of tartrazine was characterized by one band in the ultraviolet region located at 257 nm and by another band in visible region located at 428 nm. The peak at 257 nm is due to benzene-like structure in the molecules while the band in the visible region is associated with the chromophores containing azo linkage [18]. The disappearance of the absorbance peak at 428 nm with the reaction time could stem from the fragmentation of the azo links by oxidation [19]. In addition to this rapid removal effect, the decay of the absorbance at 257 nm was considered as evidence of aromatic fragment degradation in the dye molecule and its intermediates.

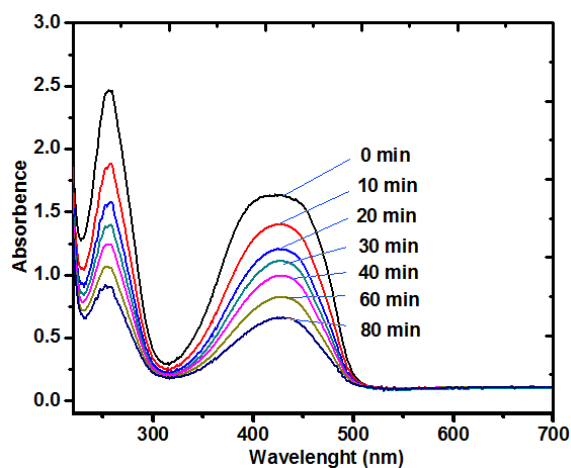
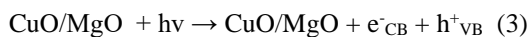


Fig. 5. UV-vis spectra of tartrazine in CuO/MgO/H<sub>2</sub>O<sub>2</sub> under UV light.

The efficiency of the prepared and characterized MgO/CuO nanocomposite was investigated for removal of Tartrazine from liquid solutions under UV radiation and H<sub>2</sub>O<sub>2</sub>. Mechanism of the photocatalytic degradation can be described as follows:



where  $h\nu$  is the UV irradiation,  $h^+_{\text{VB}}$  is valence-band holes and  $e^-_{\text{CB}}$  is the conduction-band electrons.

### 3.5. Removal of tartrazine at different conditions.

The removals of tartrazine at different conditions are presented in Fig. 6. There was no

observed loss of color for only UV or H<sub>2</sub>O<sub>2</sub>, the removal efficiencies were negligible, 4.6 and 1.5% for UV and H<sub>2</sub>O<sub>2</sub>, respectively, within 80 min. This value increased to 34.1% for the presence of both UV and H<sub>2</sub>O<sub>2</sub>, this can be ascribed to the decomposition of H<sub>2</sub>O<sub>2</sub> into hydroxyl radical (OH<sup>•</sup>), a powerful oxidizing radical, under UV irradiation.

The removal of tartrazine onto CuO/MgO was fast then reached the most saturation within 20 min, showing the removal efficiency of 35.9%. This phenomenon can be attributed to the adsorption of tartrazine if no UV was irradiated. It was smaller than the adsorption of tartrazine on pure MgO in 80 min 99.3% (the adsorption process was not presented in Fig. 6) due to the significantly decrease in surface area when CuO was added in to MgO sample. However, the removal efficiency of tartrazine in CuO/MgO/UV system was fast within initial 10 min then gradually increased in 80 min, indicating the ability reaction of tartrazine onto CuO/MgO like the photocatalyst process, as present in previous report [20].

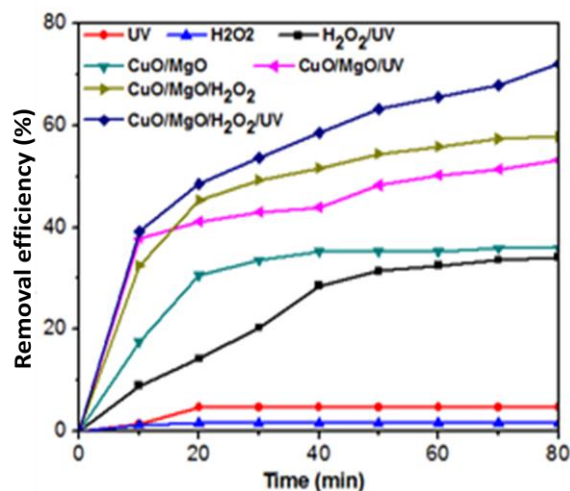


Fig. 6. Removal of dye in different conditions.

The removal of tartrazine for CuO/MgO/H<sub>2</sub>O<sub>2</sub> and CuO/MgO/H<sub>2</sub>O<sub>2</sub>/UV systems were fast within initial 20 min then gradually increased in 80 min. The removal efficiencies of CuO/MgO/H<sub>2</sub>O<sub>2</sub> was 57.7% can be attributed to the Fenton-like process [21]. Whereas, the highest removal of tartrazine in CuO/MgO/H<sub>2</sub>O<sub>2</sub>/UV systems (72.1%) can ascribed to assistant of UV in to Fenton-like system, it is expected as the Photo-Fenton-like process [21].

The reaction kinetics for photo-removal of tartrazine was investigated using pseudo 1<sup>st</sup> order kinetic model

$$\ln(C_0/C) = kt \quad (8)$$

where  $k$  (min<sup>-1</sup>) is the rate constant,  $C_0$  is the initial

concentration of tartrazine and  $C_t$  is the concentration of tartrazine in time, and  $t$  is reaction time presented by min.

Fig. 7 shows the linear relationship for  $\ln(C_0/C_t)$  plotted against irradiation time. It was evidently confirmed from the plot that photo-removal of tartrazine followed pseudo first order kinetic. The fitting equation, apparent rate constant, and  $R^2$  are presented in Table 2. The CuO/MgO catalyst showed the largest rate constant ( $0.036 \text{ min}^{-1}$ ) in the presence of  $\text{H}_2\text{O}_2$  under UV irradiation.

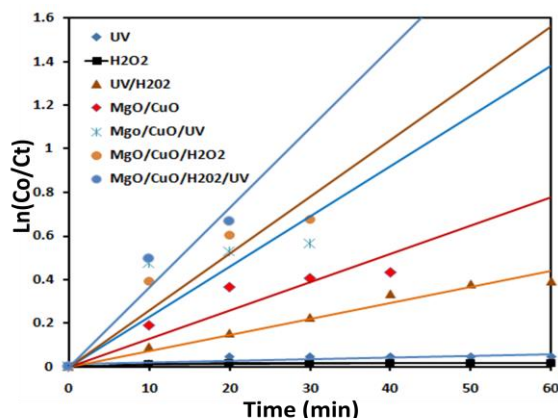


**Fig. 7.** Plots of  $\ln(C_0/C_t)$  as a function of time (min) towards the photo-removal of tartrazine under different conditions.

**Table 2.** Observed fitting of pseudo-first order equation,  $R^2$  values, rate constants, removal efficiency of tartrazine in different systems.

Reaction condition	Fitting equation	$R^2$	$k$ ( $\text{min}^{-1}$ )	Removal efficiency at 120 min (%)
$\text{H}_2\text{O}_2$	$y=0.00019x$	0.94	0.00019	1.5
UV	$y=0.00074x$	0.91	0.00074	4.6
UV/ $\text{H}_2\text{O}_2$	$y=0.0073x$	0.97	0.0073	34.1
MgO/CuO	$y=0.013x$	0.83	0.013	35.9
MgO/CuO/UV	$y=0.023x$	0.61	0.023	53.1
MgO/CuO/ $\text{H}_2\text{O}_2$	$y=0.026x$	0.87	0.026	57.7
MgO/CuO/ $\text{H}_2\text{O}_2$ /UV	$y=0.036x$	0.91	0.036	72.1

#### 4. Conclusion

The CuO/MgO composite was successfully prepared by co-precipitation method. The surface area, pore volume became much smaller, but pore size was larger than those of MgO. The removal efficiency observed was in the order: CuO/MgO/UV/ $\text{H}_2\text{O}_2$  > CuO/MgO/ $\text{H}_2\text{O}_2$  > CuO/MgO/UV > CuO/MgO > UV/ $\text{H}_2\text{O}_2$  > UV >  $\text{H}_2\text{O}_2$ . The removal of tartrazine in MgO/CuO/UV and MgO/CuO/ $\text{H}_2\text{O}_2$  can be ascribed to photocatalyst and Fenton-like reaction processes, whereas the reaction of tartrazine in

CuO/MgO/UV/ $\text{H}_2\text{O}_2$  systems with the highest reaction rate ( $0.036 \text{ min}^{-1}$ ) and the largest removal efficiency (72.1%) can be attributed to Photo-Fenton-like process. Therefore, CuO/MgO composite had great potential application for removal of dyes from wastewater.

#### References

- [1] M. Chuai, Q. Zhao, T. Yang, Y. Luo, M. Zhang, Synthesis and ferromagnetism study of Ce doped CuO dilute magnetic semiconductor, *Materials Letters* 161 (2015) 205-207.
- [2] A. Umar, A.A. Alshahrani, H. Algarni, R. Kumar, CuO nanosheets as potential scaffolds for gas sensing applications, *Sensors and Actuators B: Chemical* 250 (2017) 24-31.
- [3] M.u. haq, M. Iqbal, M.A.Z.G. Sial, S. Shabbir, M. Siddiq, A. Iqbal, Effect of Fe doping on the crystallinity of CuO nanotubes and the efficiency of the hybrid solar cells, *Journal of Photochemistry and Photobiology A: Chemistry* 335 (2017) 112-118.
- [4] R. Dang, X. Jia, X. Liu, H. Ma, H. Gao, G. Wang, Controlled synthesis of hierarchical Cu nanosheets @ CuO nanorods as high-performance anode material for lithium-ion batteries, *Nano Energy* 33 (2017) 427-435.
- [5] A. Sharma, R.K. Dutta, A. Roychowdhury, D. Das, A. Goyal, A. Kapoor, Cobalt doped CuO nanoparticles as a highly efficient heterogeneous catalyst for reduction of 4-nitrophenol to 4-aminophenol, *Applied Catalysis A: General* 543 (2017) 257-265.
- [6] A.-T. Vu, S. Jiang, Y.-H. Kim, C.-H. Lee, Controlling the physical properties of magnesium oxide using a calcination method in aerogel synthesis: Its application to enhanced sorption of a sulfur compound, *Ind. Eng. Chem. Res.* 53 (2014) 13228-13235.
- [7] T.G. Venkatesha, R. Viswanatha, Y. Arthoba Nayaka, B.K. Chethana, Kinetics and thermodynamics of reactive and vat dyes adsorption on MgO nanoparticles, *Chemical Engineering Journal* 198-199 (2012) 1-10.
- [8] R.M. Mohamed, A. Shawky, I.A. Mkhallid, Facile synthesis of MgO and Ni-MgO nanostructures with enhanced adsorption of methyl blue dye, *Journal of Physics and Chemistry of Solids* 101 (2017) 50-57.
- [9] H.R. Mahmoud, S.A. El-Molla, M. Saif, Improvement of physicochemical properties of  $\text{Fe}_2\text{O}_3/\text{MgO}$  nanomaterials by hydrothermal treatment for dye removal from industrial wastewater, *Powder Technology* 249 (2013) 225-233.
- [10] Y. Haldorai, J.-J. Shim, An efficient removal of methyl orange dye from aqueous solution by adsorption onto chitosan/MgO composite: A novel reusable adsorbent, *Applied Surface Science* 292 (2014) 447-453.

- [11] V.K. Gupta, Suhas, Application of low-cost adsorbents for dye removal – A review, *Journal of Environmental Management* 90 (2009) 2313-2342.
- [12] S. Wang, E. Ariyanto, Competitive adsorption of malachite green and Pb ions on natural zeolite, *Journal of Colloid and Interface Science* 314 (2007) 25-31.
- [13] C.R. Holkar, A.J. Jadhav, D.V. Pinjari, N.M. Mahamuni, A.B. Pandit, A critical review on textile wastewater treatments: Possible approaches, *Journal of Environmental Management* 182 (2016) 351-366.
- [14] S. Naama, T. Hadjersi, H. Menari, G. Nezzal, L.B. Ahmed, S. Lamrani, Enhancement of the tartrazine photodegradation by modification of silicon nanowires with metal nanoparticles, *Mater. Res. Bull.* 76 (2016) 317-326.
- [15] R.K. Gautam, P.K. Gautam, S. Banerjee, V. Rawat, S. Soni, S.K. Sharma, M.C. Chattopadhyaya, Removal of tartrazine by activated carbon biosorbents of *Lantana camara*: Kinetics, equilibrium modeling and spectroscopic analysis, *Journal of Environmental Chemical Engineering* 3 (2015) 79-88.
- [16] A.-T. Vu, S. Jiang, K. Ho, J.B. Lee, C.-H. Lee, Mesoporous magnesium oxide and its composites: Preparation, characterization, and removal of 2-chloroethyl ethyl sulfide, *Chemical Engineering Journal* 269 (2015) 82-93.
- [17] M. Rezaei, M. Khajenoori, B. Nematollahi, Preparation of nanocrystalline MgO by surfactant assisted precipitation method, *Materials Research Bulletin* 46 (2011) 1632-1637.
- [18] L. Singh, P. Rekha, S. Chand, Cu-impregnated zeolite Y as highly active and stable heterogeneous Fenton-like catalyst for degradation of Congo red dye, *Sep. Purif. Technol.* 170 (2016) 321-336.
- [19] Y.Z. H. Zhang, D.B. Zhang, Decolorization and mineralization of CI Reactive Black 8 by Fenton and ultrasound/Fenton method, *Color. Techno* 123 (2007) 101-105.
- [20] Q. Wang, T. Li, P. Xie, J. Ma, MgO nanolayering of Cu<sub>2</sub>O semiconductors enhances photoreactivity: Superoxide radicals boost, *Journal of Environmental Chemical Engineering* 5 (2017) 2648-2657.
- [21] N. Wang, T. Zheng, G. Zhang, P. Wang, A review on Fenton-like processes for organic wastewater treatment, *Journal of Environmental Chemical Engineering* 4 (2016) 762-787.